

Comparison of Rotor Magnetic Circuit Topologies for Passively Levitated Self-bearing Machines

Adrien ROBERT, Joachim VAN VERDEGHEM, Bruno DEHEZ

*Mechatronic, Electrical Energy, and Dynamic Systems (MEED),
Université catholique de Louvain (UCLouvain), Louvain-la-Neuve, Belgium.
Emails: {adrien.robert, joachim.vanverdegheem, bruno.dehez}@uclouvain.be*

Abstract

Self-bearing motors can reach high rotation speeds thanks to the rotor magnetic levitation. In order to improve the compactness of such a motor, a fully passive levitation achieved with an electrodynamic thrust bearing has recently been proposed and studied. However, the proposed topologies do not integrate magnetic circuit in the rotor, or only at a significant distance from the winding, although it can improve the performance of the motor and the suspension through the impact it can have on the inductance coefficients of the winding. In this context, this paper aims to compare different rotor magnetic circuits topologies on the performance of axial flux self-bearing motors based on electrodynamic suspensions.

Keywords: Self-bearing motor, Electrodynamic suspension, Magnetic circuit.

1. Introduction

Self-bearing machines combine the drive and magnetic suspension functions in a single structure, making them ideal for applications requiring high rotation speed and power density (Chen et al. 2020, Pei et al. 2022). These motors use active methods to ensure magnetic levitation along each degree of freedom (DOF), which requires sensors, controllers and power electronics to operate. Reducing the number of actively controlled DOFs is therefore one of the current challenges for self-bearing motors to improve their compactness, reliability and cost. From this perspective, recent research has proposed theoretical and experimental studies of fully passively levitated self-bearing motors, with axial (Van Verdegheem & Dehez 2021) and radial (Rubio et al. 2023) flux topologies, based on an Electrodynamic Thrust Self-Bearing Machine (ETSBM). Both are based on a Surface-Mounted Permanent Magnet (SMPM) rotor whose ferromagnetic parts are located at such a distance from the winding that they almost do not affect the inductance coefficient. However, the presence of a magnetic circuit could have a positive impact on the ETSBM performance by increasing the winding inductance, which directly determines the electrodynamic suspension force at low speed, and making it dependent on the rotor position.

On these premises, a model that takes into account the impact of the ferromagnetic circuit on the dynamic behaviour of the motor, through the evolution of the inductance coefficients with the axial and angular positions of the rotor, has recently been proposed (Robert et al. 2023, Van Verdegheem et al. 2022). In addition to the new reluctant torque created by the saliencies, it reveals the appearance of new reluctant and cross terms in the expression of the axial stiffness, which could lead to a suspension force modulation through the injection of d-axis current. A simplified variant of this model has been derived to investigate the impact of ferromagnetic yokes called Back Iron (BI) (Van Verdegheem et al. 2022), attached to the axial flux rotor behind the armature winding. It shows an effective improvement of the driving torque, but the investigated topology is without magnetic saliencies. In this context this paper aims to evaluate the impact of such saliencies on the motor and suspension performance of the ETSBM.

2. General principle

The general structure of the ETSBM and its working principle are depicted in Figure 1. When the rotor is axially centred (Figure 1(a)), the PM flux linkages of the upper and lower windings are equal, which means that the motor current I_M , injected by the power supply, is evenly distributed between both windings. Due to the machine symmetry, this current generates only a driving torque $T_{\theta,M}$, regardless of the axial position of the rotor.

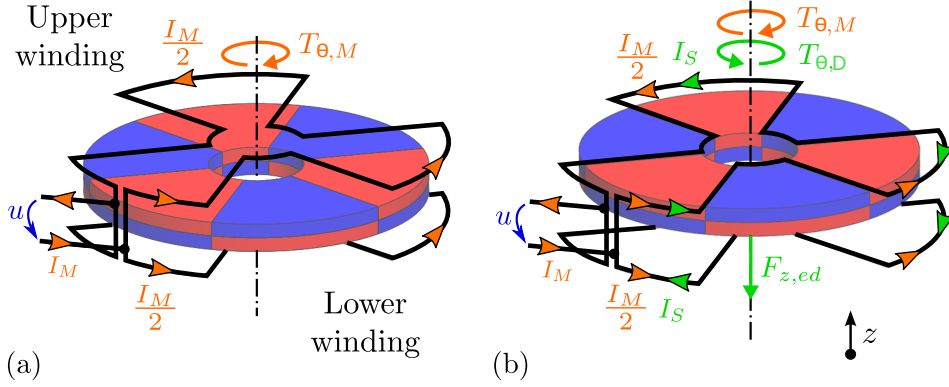


Figure 1: ETSBM operation, ironless topology and only one phase represented. (a) Centered position ($z = 0$). (b) Decentered position ($z \neq 0$). Inspired from (Van Verdegheem & Dehez 2021).

In the case of an axial displacement of the rotor (Figure 1(b)), a suspension current I_S arises due to the imbalance in both the back electromotive force and the impedance between the upper and lower windings. The different circulation direction of this current induces an axial restoring force F_z as well as a parasitic torque $T_{\theta,D}$ that is superimposed on the driving one. This parasitic component is also called "drag torque" because it is generally opposed to the driving torque.

3. Performance criteria

The restoring force depends linearly on the axial displacement, which allows to define an axial stiffness k_z . Its general expression, given below in the Park-Concordia frame, has been introduced in (Robert et al. 2023):

$$k_z = \frac{\omega^2}{\omega_e^2 + \omega^2} \cdot \underbrace{\left(\frac{3K_{\theta,z}^2}{L_{S,d}} + \sqrt{6} \cdot K_{\theta,z} \cdot \frac{L_{d,z}}{L_{S,d}} \cdot I_{M,d} + \frac{L_{d,z}^2}{2L_{S,d}} \cdot I_{M,d}^2 + \frac{L_{q,z}^2}{2L_{S,q}} \cdot I_{M,q}^2 \right)}_{k_z^\infty} \quad (1)$$

The stiffness depends on the direct and quadrature motor currents $I_{M,d}$ and $I_{M,q}$, the direct and quadrature suspension inductance $L_{S,d}$ and $L_{S,q}$, the axial gradient of the latter $L_{d,z}$ and $L_{q,z}$, the axial gradient of the flux amplitude $K_{\theta,z}$, the rotation speed ω , and the electrical pole defined as $\omega_e = \frac{R}{p\sqrt{L_{S,d} \cdot L_{S,q}}}$ with the phase resistance R and the pole pair number p .

Equation 1 shows that the axial force increases with the rotation speed up to reach its asymptotic value k_z^∞ . The first component of this asymptotic stiffness is the electrodynamic one and is the only force component acting in ironless ETSBM. As soon as the rotor contains a ferromagnetic circuit, the inductance coefficients vary with the axial position, creating additional stiffness components which depend on the motor currents. Therefore, an ETSBM with a ferromagnetic circuit adds a possibility of stiffness modulation through the variation of the load angle α_{load} , unlike to the ironless motor where the suspension is completely independent from the power supply.

The suspension performance of an ETSBM can be evaluated using two terms. First, the asymptotic stiffness k_z^∞ defined in Equation 1, which is the maximum reachable stiffness. Second, the electrical pole ω_e , representative of the stiffness evolution: the lower the electrical pole, the faster the stiffness reaches its asymptotic stiffness and then the higher the suspension at low speed. Therefore, significant suspension performance results from a combination of an important asymptotic stiffness and a small electrical pole.

The general expression of the total torque developed by the motor is the following:

$$T_\theta = \underbrace{\sqrt{\frac{3}{2}} p \cdot I_{M,q} K_\theta + p \cdot \frac{I_{M,q} I_{M,d}}{2} \cdot (L_{M,d} - L_{M,q})}_{T_{\theta,M}} + T_{\theta,D}(z^2, \omega) \quad (2)$$

where are introduced the flux amplitude in centered position K_θ and the direct and quadrature motor inductances $L_{M,d}$ and $L_{M,q}$. As stated in Section 2, the total torque is composed of the driving torque $T_{\theta,M}$ and a parasitic torque $T_{\theta,D}$. This latter evolves with the rotation speed up to reach an asymptotic value and is proportional to the square of the rotor axial displacement. For clarity reason, its expression is not developed here but can be found in (Robert et al. 2023). In centered position, the only existing torque is therefore the driving one, composed of the classical electrodynamic and reluctant torque components.

4. Investigated topologies

Two rotor topologies are investigated, the classical SMPM and the Spoke Type Permanent Magnet (STPM). Both topologies, represented in Figure 2 with their characteristic dimensions, are studied with and without a back-iron (BI), the latter being part of the rotor to avoid an axial detent force resulting in a negative stiffness.

5. Methodology

The comparison of the different topologies presented previously is based on the two performance criteria of Section 3., the torque in centered position and the asymptotic stiffness. To that end, a NSGA-II algorithm is used to optimise each topology according to both criteria. These bi-objective optimisations are performed constraining the Joule losses P_J , the PM volume V_{PM} , and the load angle α_{load} . Equations 1 and 2 require the flux and inductance coefficients which are obtained through 3D FEM simulations. The parameters used in the optimisation are summarised in Table 1.

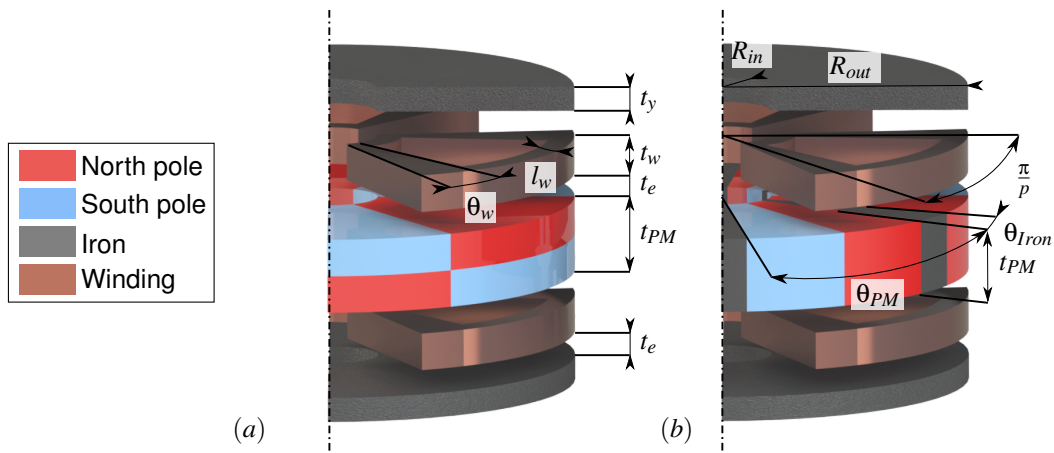


Figure 2: Dimension parameters for both topologies with back-iron, only one phase represented (a) Surface mounted permanent magnet rotor (b) Spoke type rotor.

Parameter	Symbol	Unit	Value for		Parameter	Symbol	Unit	Value for	
			SMPM	STPM				SMPM	STPM
Optimized parameters									
Number of pole pairs	p	-	[15,40]		Winding thickness	t_y	mm	[3,8]	
Outer radius	R_{out}	mm	[20,150]		Inner radius	R_{in}	mm	[10,90]	
PM angular opening	θ_{PM}	rad	/	$\left[\frac{1}{10} \frac{\pi}{p}, \frac{4}{5} \frac{\pi}{p} \right]$					
Fixed parameters									
Back iron thickness	t_y	mm	7.5		Air gap thickness	t_e	mm	0.75	
Angular opening coefficient of windings	c_o	-	0.75		Number of phase	N	-	3	
Joule losses	P_j	W	12.5		Load angle	α_{load}	rad	$\frac{\pi}{2}$	
Volume of PM	V_{PM}	cm ³	5						
Depending parameters									
Iron angular opening	θ_{Iron}	rad	/	$\frac{\pi}{p} - \theta_{PM}$	Iron thickness	t_{PM}	mm	$\frac{V_{PM}}{\pi \cdot (R_{out}^2 - R_{in}^2)}$	$\frac{V_{PM}}{p \cdot \theta_{PM} \cdot (R_{out}^2 - R_{in}^2)}$
Winding angular opening	θ_w	rad		$c_o \cdot \frac{\pi}{N \cdot p}$	Winding width	l_w	mm	$R_{in} \cdot \frac{\theta_w}{1 - \theta_w}$	

Table 1: Optimizations parameters of both topologies

6. Results

The comparison is first made on the asymptotic stiffness directly provided by the optimization algorithm, and therefore investigated on the full speed range.

6.1 Comparison on asymptotic stiffness

Preliminary analysis can be made on the Pareto fronts obtained from the optimisation process and shown in Figure 3. They reveal that the SMPM and STPM topologies reach quite the same suspension performance when they are optimised for torque in the range of 0.25 Nm, but that BI has a global negative impact.

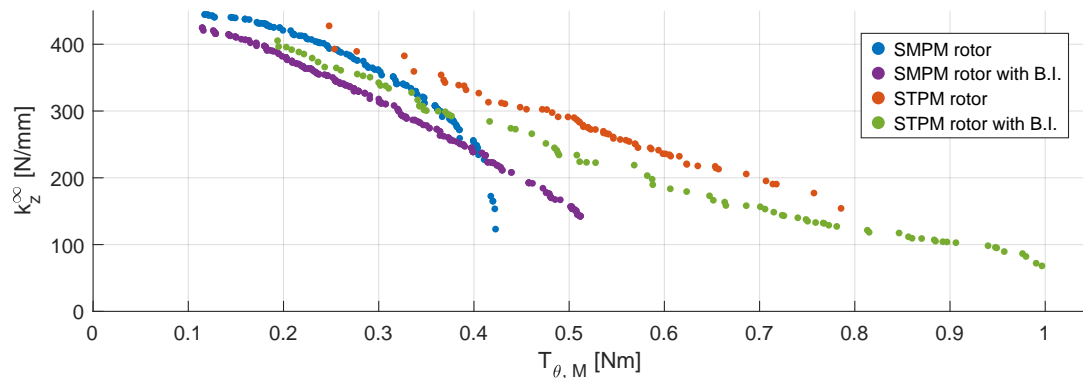


Figure 3: Pareto fronts reached for each topology at fixed permanent magnet volume and Joule losses.

When optimised for higher torques, both the SMPM and the STPM topologies without BI have a faster decrease in asymptotic stiffness than those with BI, to the point where they become less efficient at high torques. However, compared to SMPM, the STPM topologies without BI perform better as keep their advantage over topologies with BI for larger torque ranges.

Conversely, when optimised for lower torques, both the SMPM and the STPM topologies without BI see their suspension performance criteria increase less rapidly than those with BI, so that they tend to become less performant at low torque. When comparing STPM and SMPM and without taking into account the presence of BI, the first topology still provides better asymptotic suspension than SMPM one for a given torque. However, SMPM topologies reach wider low torque range, where the best suspension performances are obtained.

These results also show that topologies with BI outperform their counterparts without BI in terms of the maximum torque they can generate, as well as STPM topologies compared to SMPM. the opposite is true for the maximum reachable suspension: the topologies without BI perform better, especially the SMPM one.

6.2 Comparison on full speed range

Previous observations have been made considering the asymptotic stiffness, whereas the stiffness at the nominal operating point is intrinsically dependent on the speed and the electrical pole, as established by Equation 1. Then the question may arise as to whether these observations remain valid regardless of the speed regime. Figures 4(a) and 4(b) show, respectively for the topologies without and with BI, the evolution of the stiffness of the different machines of the Pareto front as a function of the operating speed. Moreover Figures 4(c) and 4(d) show the evolution of the stiffness difference Δk_z between the STPM and SMPM topologies for common torque range of both topologies and in parallel with the evolution of their electrical poles ω_e .

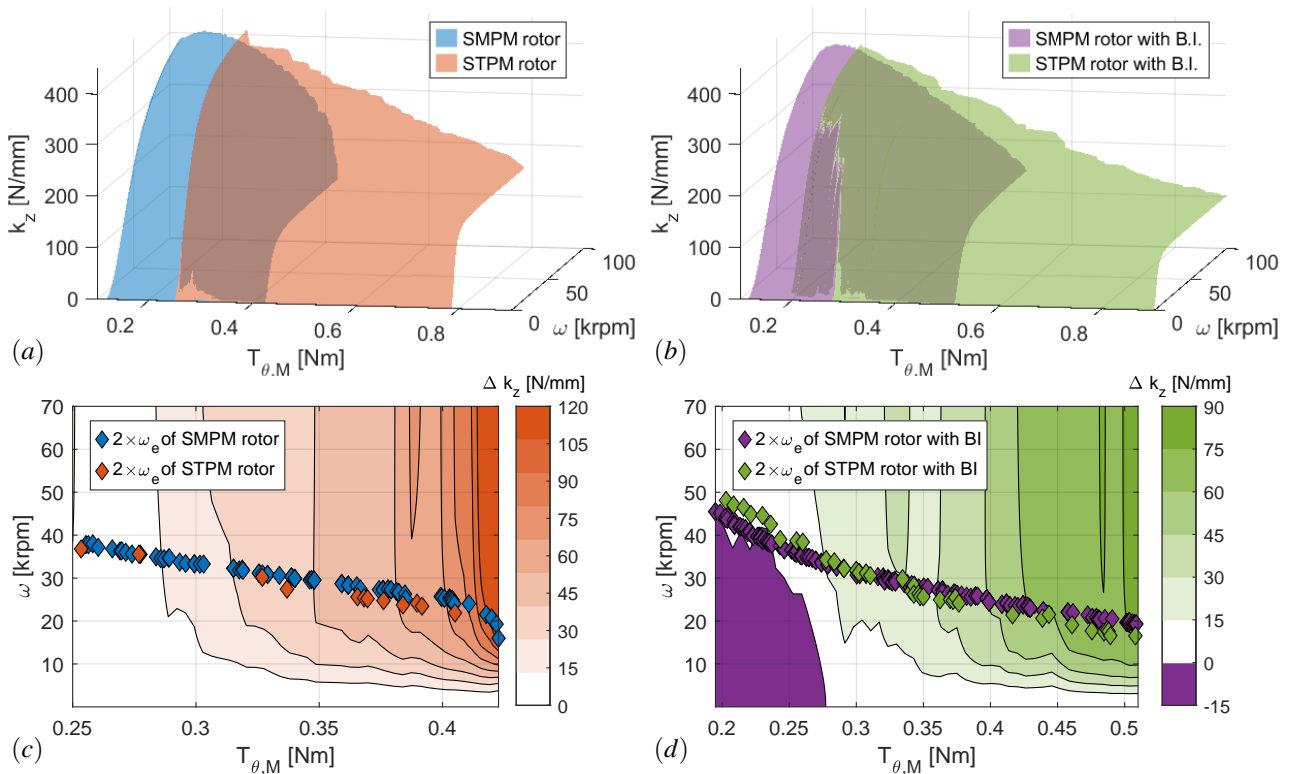


Figure 4: (a) and (b) Evolution of the stiffness with the rotation speed for Pareto front motors of SMPM and STPM topologies, respectively without and with BI, for rotation speed up to 100 [krpm]. (c) and (d) Difference in stiffness between the STPM and SMPM topologies, respectively without and with BI, for rotation speed up to 70 [krpm] and torque range achieved by both topologies. Both also show double the value of the electrical poles ω_e of each Pareto front.

Figures 4(a) and (c) reveal that the observations made on topologies without BI are still valid: for the torque range achieved by both topologies, the STPM always provides the best suspension capability. They also validate the principle of optimising and comparing both topologies based on asymptotic stiffness.

However, for topologies with BI optimised for the low torque range, the SMPM achieves a higher stiffness than STPM when the rotation speed does not exceed 50 krpm. This is explained by the lower value of the electrical pole of the SMPM topology for these low torque, as shown in Figure 4(d). For torques higher than 0.28 Nm, STPM topology combines higher asymptotic stiffness and lower electrical pole, which ensures better suspension performance than SMPM over the whole speed range.

7. Conclusion

An optimisation process, aiming to maximize the torque and asymptotic stiffness of an ETSBM, was applied to different rotor topologies with fixed permanent magnet volume and Joule losses. This showed that STPM topologies performed better for applications requiring high torque, while SMPM topologies performed better for applications requiring high stiffness. In addition, it also revealed that topologies without BI achieved a better compromise between torque and stiffness than those with BI. Furthermore, a study of the impact of speed on the induced stiffness achieved by both topologies in the common torque range showed that the STPM topology always provides the best suspension capability except in one case, for topology with BI at low rotation speed and torque, where the SMPM topology provides greater stiffness thanks to their lower electrical pole. Future work will investigate the influence of the different geometric parameters as well as the impact of the load angle, which could exploit the ferromagnetic saliencies to increase the torque capability of the STPM rotor.

Acknowledgement

This publication is supported by "La Région wallonne" as part of the funding of a FRIA grant.

References

- Chen, J., Zhu, J. & Severson, E. L. (2020), 'Review of Bearingless Motor Technology for Significant Power Applications', *IEEE Transactions on Industry Applications* **56**(2), 1377–1388.
- Pei, T., Li, D., Liu, J., Li, J. & Kong, W. (2022), 'Review of Bearingless Synchronous Motors: Principle and Topology', *IEEE Transactions on Transportation Electrification* **8**(3), 3489–3502.
- Robert, A., Herrman, S., Van Verdegheem, J. & Dehez, B. (2023), 'Dynamical Modeling of Passively Levitated Electrodynamic Thrust Self-Bearing Machines considering impact of ferromagnetic circuit', *To be submitted to IEEE Transaction on Magnetics*.
- Rubio, G. C., Hothur Komal, V. C., Fujii, Y. & Chiba, A. (2023), 'Experimental Verification of Passive Axial Electrodynamic Suspension in a Bearingless Motor', *IEEE Open Journal of Industry Applications* pp. 1–12.
- Van Verdegheem, J. & Dehez, B. (2021), 'Fully Passively Levitated Self-Bearing Machine Implemented Within a Reaction Wheel', *IEEE Transactions on Industry Applications* **57**(6), 5782–5795.
- Van Verdegheem, J., Robert, A., Herrman, S. & Dehez, B. (2022), Impact of Ferromagnetic Yokes on Axial Flux Passively Levitated Self-Bearing Machines, in '2022 25th International Conference on Electrical Machines and Systems (ICEMS)', pp. 1–6.